Dynamic thermo-mechanical properties of shape memory alloy nanowires upon multi-axial loading

Dhote, R. P., Melnik, R. V. N., Zu, J. W.

Proceedings of the ASME 2011 Conference on Smart Materials, Adaptive Structures and Intelligent Systems (SMASIS-2011), Sept 18 - 21, 2011, Scottsdale, AZ, USA, Volume 2, Paper SMASIS2011-5210, pp. 411--417,

ISBN 978-0-7918-5472-3, 2011.

Proceedings of the ASME 2011 Conference on Smart Materials, Adaptive Structures and Intelligent Systems
SMASIS2011
September 18-21, 2011, Scottsdale, Arizona, USA

SMASIS2011-5210

DYNAMIC THERMO-MECHANICAL PROPERTIES OF SHAPE MEMORY ALLOY NANOWIRES UPON MULTI-AXIAL LOADING

Rakesh P. Dhote *
Dept. of Mechanical and Industrial Engg.
University of Toronto
5 King's College Road
Toronto, Canada M5S 3G8
Email: rakesh.dhote@utoronto.ca

Roderick V.N. Melnik
M^2NeT Laboratory
Wilfrid Laurier University
Waterloo, Canada, N2L 3C5

Jean W. Zu
Dept. of Mechanical and Industrial Engg.
University of Toronto
5 King's College Road,
Toronto, Canada M5S 3G8

ABSTRACT

In this paper, we study the behavior of shape memory alloy (SMA) nanowires subjected to multi-axial loading. We use the model developed in our earlier work to study the microstructure and mechanical properties of finite length nanowires. The phase field model with the Ginzburg-Landau free energy is used to model the phase transformation based on the chosen order parameter. The governing equations of the thermo-mechanical model are solved simultaneously for different loading cases. We observe that nanowire behaves in a stiff manner to axial load with complete conversion of the unfavorable martensite to the favorable one. The bending load aids the phase transformation by redistributing the martensitic variants based on the local axial stress sign. The nanowire behavior to multi-axial (axial and bending together) is stiffer axially than the axial loading case. The understanding of the behavior of nanowire to multi-axial loading will be useful in developing better SMA- based MEMS and NEMS devices.

INTRODUCTION

The nanowires have been extensively studied over last two decades for their potential applications in nano- and bio- technology devices for various applications including nanomanipulation, nanoassembly, and material characterization. These applications require displacement in nanometer range and forces in nano-Newton range. The SMA nanowires are promising candidate to meet these requirements. SMAs have temperature dependent mechanical properties, microstructure and possess ability to change their shape based on thermal and mechanical loadings. They inhabit an ideal combination of high energy density and large strain properties. Despite these advantages, SMAs find more limited applications than their piezoelectric counterparts because of low actuation frequency [1]. The reason for low actuation frequency is physical limitations of heat transfer between the SMA and its surrounding. The heat transfer in SMA can be enhanced either by using a material with high heat transfer coefficient or increasing the surface area of a SMA structure. The use of material with high heat transfer material is not a viable option as SMA properties are very sensitive to its constituent combinations. The practical method of increasing the actuation frequency is to increase a surface area. One of the possible ways to do that is to reduce the structure dimensions to nanoscale where the surface-to-volume ratio becomes very high. By changing SMA structure dimensions at the nanoscale, the heat transfer could be changed and the SMA nanowire can be used in a range of potential applications such as MEMS and NEMS technologies [2, 3], biomechanical and medicine applications [4–6], etc.

Several models have been developed to study the SMA behavior across different length scales [7]. The phase field (PF) models have been used to study microstructure and mechanical properties of nanoscale SMA specimens. Bouville et al. [8] used the PF model with the Ginzburg-Landau free energy to study

*Address all correspondence to this author.

the microstructure in constrained nanostructures and mechanical properties of infinite length nanowires upon axial loading. Ahluwalia et al. [9] carried out the three dimensional simulations to study the axial properties of nanosize samples with periodic boundary conditions for the cubic-to-tetragonal phase transformations in the FePd crystals. Idesman et al. [10] studied the evolution of microstructures in periodic nanosize three dimensional NiAl samples using the advanced potential developed by Levitas et al. [11–13]. All the above simulations have been carried out under the assumption of isothermal or athermal conditions, although SMAs possess strong temperature dependent properties. Furthermore, all the studies focused on the behavior of SMA nanostructures under axial loading only. However, multiaxial loading conditions may be induced in the nanowire during interaction with its environment. It is important to study the thermo-mechanical behavior of SMA nanowires under multi-axial loading accounting for the fully coupled thermo-mechanical model.

In this contribution, we study the properties of finite length nanowires with fully coupled nonlinear thermo-mechanical formulation under multi-axial loadings. We first setup the model of SMA dynamics based on the Ginzburg-Landau free energy for the square-to-rectangular phase transformations, evolve the microstructure and then perform numerical experiments to study the thermo-mechanical properties under multi-axial loadings as described in the following sections.

SMA DYNAMICS

We setup the mathematical model for SMA dynamics based on the mesoscale model analyzed in detail numerically in our earlier work [14, 15]. In this paper, we study the mechanical behavior in FePd nanowires. The FePd material has high temperature, high symmetry face centered cubic (FCC) austenite phase and low temperature, low symmetry face centered tetragonal (FCT) martensitic phases (with tetragonal crystal aligned with elongated side along three rectilinear directions). The material exhibits cubic-to-tetragonal phase transformations under thermal and mechanical loadings. The phase transformation is a highly nonlinear phenomenon. In addition the coupled thermo-mechanical modeling and three dimensional simulations make computations challenging.

To make the computations tractable, we study the behavior of nanowires using the simplified two dimensional square-to-rectangular representative phase transformations, where the square represents the austenite phase A and the rectangles represent the martensitic variants $M+$ and $M-$ (with rectangle length aligned along two perpendicular axes). As the austenite and martensite variants have different energies and exist at different temperature, the phase transformations in SMA can be modeled by using the Ginzburg-Landau free energy defined with reference to the austenite phase. The free energy function $\mathscr{F}$ for the SMA dynamics can be defined in terms of the symmetric strain tensor as

$$\begin{aligned}
\mathscr{F}(\theta,e_i) &= \mathscr{F}_e(e_i)+\mathscr{F}_{pt}(\theta,e_2)+\mathscr{F}_g(\nabla e_2),\\
\mathscr{F}_e(e_i) &= \frac{a_1}{2}e_1^2+\frac{a_3}{2}e_3^2,\\
\mathscr{F}_{pt}(\theta,e_2) &= \frac{a_2}{2}\left(\frac{\theta-\theta_m}{\theta_m}\right)e_2^2-\frac{a_4}{4}e_2^4+\frac{a_6}{6}e_2^6,\\
\mathscr{F}_g(\nabla e_2) &= \frac{k_g}{2}\left[\left(\frac{\partial e_2}{\partial x}\right)^2+\left(\frac{\partial e_2}{\partial y}\right)^2\right],
\end{aligned} \tag{1}$$

where e_1, e_2 and e_3 are the hydrostatic, deviatoric and shear strain respectively defined as
$e_1=(\varepsilon_{xx}+\varepsilon_{yy})/\sqrt{2}$, $e_2=(\varepsilon_{xx}-\varepsilon_{yy})/\sqrt{2}$, $e_3=(\varepsilon_{xy}+\varepsilon_{yx})/2$, with $\varepsilon_{ij}=[(\partial u_i/\partial x_j)+(\partial u_j/\partial x_i)]/2$ being the Cauchy-Lagrange strain tensor (with the repeated index convention used); u_i, $\mathrm{i}=1,2$ are displacements along x and y directions respectively, θ is the material temperature, θ_m is the austenite-martensite phase transformation temperature, a_i are the material constants, and k_g is the Ginzburg coefficient.

The $\mathscr{F}_e$ term in Eqn. 1 is the elastic energy which stabilizes the twinned microstructure [16]. The phase transformation energy $\mathscr{F}_{pt}$ defines the first order phase transformations and the gradient energy $\mathscr{F}_g$ introduces non-local effects and prevents a system from creating infinite number of interfaces.

The deviatoric strain e_2 is selected as the order parameter to distinguish different phases in a domain. The austenite phase exists when $e_2=0$ ($\frac{\partial u_1}{\partial x}=\frac{\partial u_2}{\partial y}$), the martensite variants $M+$ when $e_2>0$ ($\frac{\partial u_1}{\partial x}>\frac{\partial u_2}{\partial y}$), and the martensite variant $M-$ when $e_2<0$ ($\frac{\partial u_1}{\partial x}<\frac{\partial u_2}{\partial y}$).

The SMA is in the austenite phase when temperature θ is above the transformation temperature θ_m. The martensite variants exist when temperature is below θ_m, and the state degenerates with the austenite and the martensite variants appearing simultaneously when $\theta\approx\theta_m$. With the free energy given by Eqn. 1, the SMA behavior is captured by building the mathematical model that couples the structural and thermal fields using the conservation equations of mass, momentum, and energy in the way described previously in [17]. The structural (or mechanical) field equation is written as

$$\rho\frac{\partial^2 u_i}{\partial t^2}=\sum\frac{\partial\sigma_{ij}}{\partial x_j}+\sigma_{g_i}+\eta\nabla^2 v_i+f_i, \tag{2}$$

where ρ is the mass density, v_i is the time derivative of displacement u_i, η is the damping coefficient, $\sigma_{ij}=\frac{\partial}{\partial\varepsilon_{ij}}(\mathscr{F}_e+\mathscr{F}_{pt})$, and $\sigma_{g_i}=\frac{\partial\mathscr{F}_g}{\partial\varepsilon_{ij}}$. On simplification, we obtain the stress tensor com-

ponents as

$$\sigma_{11} = \frac{1}{\sqrt{2}}\left[a_1 e_1 + a_2\left(\frac{\theta-\theta_m}{\theta_m}\right)e_2^2 - a_4 e_2^3 + a_6 e_2^5\right],$$
$$\sigma_{12} = \frac{1}{2}a_3 e_3 = \sigma_{21},$$
$$\sigma_{22} = \frac{1}{\sqrt{2}}\left[a_1 e_1 - a_2\left(\frac{\theta-\theta_m}{\theta_m}\right)e_2^2 + a_4 e_2^3 - a_6 e_2^5\right],$$
$$\sigma_{g_1} = k_g\left[\frac{\partial^4 u_1}{\partial x^4} + \frac{\partial^4 u_1}{\partial x^2 \partial y^2} - \frac{\partial^4 u_2}{\partial x^3 \partial y} - \frac{\partial^4 u_2}{\partial x \partial y^3}\right],$$
$$\sigma_{g_2} = k_g\left[-\frac{\partial^4 u_1}{\partial x^3 \partial y} - \frac{\partial^4 u_1}{\partial x \partial y^3} + \frac{\partial^4 u_2}{\partial x^2 \partial y^2} + \frac{\partial^4 u_2}{\partial y^4}\right]. \quad (3)$$

The governing equation of the energy balance is derived based on the Cattaneo-Vernotte relationship described in [17, 18] as

$$\rho c_v \frac{\partial \theta}{\partial t} = \kappa\left(\frac{\partial^2 \theta}{\partial x^2} + \frac{\partial^2 \theta}{\partial y^2}\right) + a_2 \theta e_2 \frac{\partial e_2}{\partial t} + g, \quad (4)$$

where c_v is the specific heat constant, κ is the thermal conductivity of the material, and g is the thermal load. The dynamics can now be modeled by solving Eqn. 2 and Eqn. 4 simultaneously. These equations are first rescaled and then solved numerically by using the finite element method. Several numerical challenges have to be overcome to solve the resulting highly nonlinear system of coupled equations.

NUMERICAL SIMULATIONS

In order to study the behavior of nanowires under multi-axial loadings, a series of numerical experiments have been performed on the nanowires. The rectangular nanowires of dimension 1000×200 nm are modeled with sides parallel to $< 10 >$ and $< 01 >$ directions defined with reference to the austenite phase as shown in Fig. 1. The material parameters used for the simulations are found in [8], in particular:
$a_1 = 140$ GPa, $a_3 = 280$ GPa, $a_2 = 212$ GPa, $a_4 = 17 \times 10^3$ GPa, $a_6 = 30 \times 10^6$ GPa, $\theta = 250$ K , $\theta_m = 265$ K, $\eta = 0.025$, $k_g = 3.5 \times 10^{-8}$, $C_v = 350$ Jkg^{-1}K^{-1}, and $\kappa = 78$ Wm^{-1}K^{-1}.

Microstructure Evolution

The mechanical properties of nanowire depend on the microstructure. The simulation procedure adopted here is to first evolve the microstructure and perform the multi-axial loading test on the evolved microstructure. The microstructure is evolved by allowing the nanowire in the austenite phase $\theta > \theta_m(265\,\text{K})$ to evolve by quenching to temperature $\theta = 250$ K with the following boundary and initial conditions:

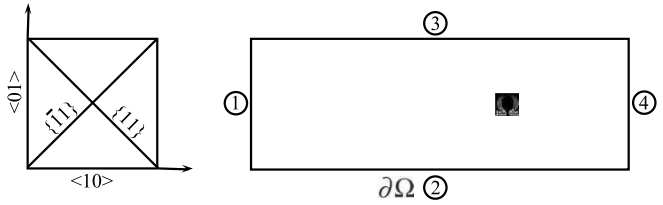

FIGURE 1: Direction, plane, and boundary ($\partial\Omega$) nomenclature in the nanowire domain (Ω)

FIGURE 2: (Color online) Evolution of microstructure in the nanowire (red and blue indicate martensite variants and green indicates austenite)

$$u_i|_{(\partial\Omega,t)} = 0, \quad \nabla u_i \cdot \mathbf{n}|_{(\partial\Omega,t)} = 0, \quad \nabla\theta \cdot \mathbf{n}|_{(\partial\Omega,t)} = 0,$$
$$\theta|_{(\Omega,t=0)} = 250\,\text{K}, \quad \dot{u}_i|_{(\partial\Omega,t)} = 0, \quad \dot{\theta}|_{(\partial\Omega,t)} = 0,$$
$$u_i|_{(\Omega,t=0)} = \text{White noise}, \quad (5)$$

where $\mathbf{n}$ is the normal vector to the boundary.

The microstructure is allowed to evolve till it gets stabilized. The evolved microstructure is shown in Fig. 2. The evolved microstructure has domain walls oriented in $\{11\}$ or $\{\bar{1}1\}$ planes to minimize the energy. During the microstructure evolution, the temperature increase is observed due to friction of atomic layers on each other during formation of the martensitic twin microstructure and due to the insulated boundary conditions.

Multi-Axial Loading

We now perform the multi-axial loading simulations on the evolved microstructure from the previous subsection. The three loading cases are considered here: axial, bending, and multi-axial (axial and bending together). The initial and boundary conditions for these simulations are:
$u_i|_{(\partial\Omega=1,t)} = 0$, $\nabla u_i \cdot \mathbf{n}|_{(\partial\Omega,t)} = 0$, $\nabla\theta \cdot \mathbf{n}|_{(\partial\Omega,t)} = 0$,
and the loading conditions for three cases are

$$\text{Axial}: u_1|_{(\partial\Omega=4,t)} = \text{d}_{\text{LU}}$$
$$\text{Bending}: u_2|_{(\partial\Omega=4,t)} = \text{d}_{\text{LU}}$$
$$\text{Multi}-\text{axial}: u_1|_{(\partial\Omega=4,t)} = \text{d}_{\text{LU}}, u_2|_{(\partial\Omega=4,t)} = \text{d}_{\text{LU}}, \quad (6)$$

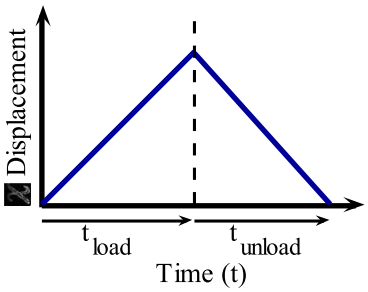

FIGURE 3: Displacement based ramp loading and unloading

where d_{LU} is the displacement based ramp loading and unloading as shown in Fig. 3 with χ displacement. The expression for displacement based ramp loading and unloading is

$$d_{LU} = \chi \left[t_{load} - |t - t_{load}| \right]. \tag{7}$$

The simulations are performed for each loading case individually. Figures 4-6 show snapshots of microstructure evolution at different time steps starting from the initial microstructure shown in Fig. 2. In the axial loading case, the phase transformation takes place during loading and unloading as shown in Fig. 4. As the nanowire is axially stretched $\frac{\partial u_1}{\partial x} > \frac{\partial u_2}{\partial y}$, the unfavored martensite ($M-$ shown in blue) is converted to favored martensite ($M+$ shown in red). This process of phase transformation to the favored martensite variant ($M- \rightarrow M+$) under loading is called as the reorientation or detwinning. The detwinning starts from the boundary 4 and travels along the negative $< 10 >$ axis with a deformation wave. As the deformation travels, the $M-$ martensite variant moves along $\{11\}$ or $\{\bar{1}1\}$ plane across the boundaries 2 and 3. The whole nanowire is transformed into the axially favorable $M+$ martensite variant with detwinning and elastic loading occurring simultaneously. Once the nanowire is fully transformed into the favorable martensite, it is loaded elastically during the rest of the loading. During the unloading part, the nanowire is first elastically unloaded before the appearance of first $M-$ variant near the constrained boundary 1. As $\frac{\partial u_1}{\partial x} < \frac{\partial u_2}{\partial y}$, the domains of $M-$ appear at the boundaries 1 and 4. At the end of unloading, the domains of both $M+$ and $M-$ exist in the nanowire. It is noted that the microstructure distribution at the end of unloading (refer to Fig. 4-(v)) is different from the initial microstructure before axial loading (refer to Fig. 2).

The microstructure evolution during the bending case is shown in Fig. 5. It is observed that the bending load causes a redistribution of the martensite variants in the nanowire during loading and unloading based on the local axial stress (σ_{xx}) sign. During loading, the $M+$ variant is redistributed to form domains at boundary 2 as σ_{xx} has positive sign, and $M-$ variant is redistributed to form domains at boundary 3 as σ_{xx} has negative sign.

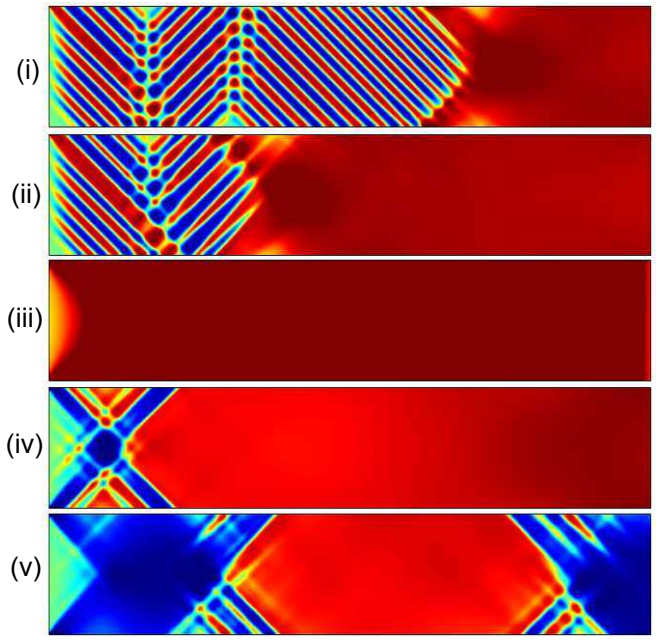

FIGURE 4: (Color online) Evolution of microstructure in the nanowire subjected to axial loading and unloading at time (ns) (i) 0.25, (ii) 0.5, (iii) 1.0, (iv) 1.5, and (v) 2.0 (red and blue indicate martensite variants and green indicates austenite)

These domains switch positions during unloading as local σ_{xx} switches sign at the boundaries 2 and 3.

The microstructure evolution in the multi-axial case is a result of combination of axial and bending loadings as shown in Fig. 6. The detwinning and redistribution of martensitic variants occur simultaneously. However, the speed of detwinning is fast due to the axial and bending load occurring simultaneously. The traces of austenite are observed at the boundaries 1 and 4.

The microstructures evolution during different loadings can be quantitatively studied by comparing the normalized area of different phases in the domain with the parameter $\hat{A}$ defined as

$$\hat{A} = \frac{\text{Area of the martensite phase}}{\text{Area of the nanowire}}. \tag{8}$$

Figure 7 shows the evolution of $\hat{A}$ for $M+$ and $M-$ variants for three loading cases. In the axial loading, the detwinning phase transformation is observed by $\hat{A}_{M+}$ reaching value 1 and $\hat{A}_{M-}$ reaching value 0 at around 0.7 ns (completed detwinning phase transformation). During the detwinning, the slope of $\hat{A}_{M+}$ is positive and the phase transformation and the elastic loading takes place simultaneously. Once the detwinning is complete, the nanowire is elastically loaded as indicated by the zero slope of $\hat{A}_{M+}$. During unloading part, the appearance of first $M-$ is observed when the $\hat{A}_{M+}$ slope becomes negative. In the case

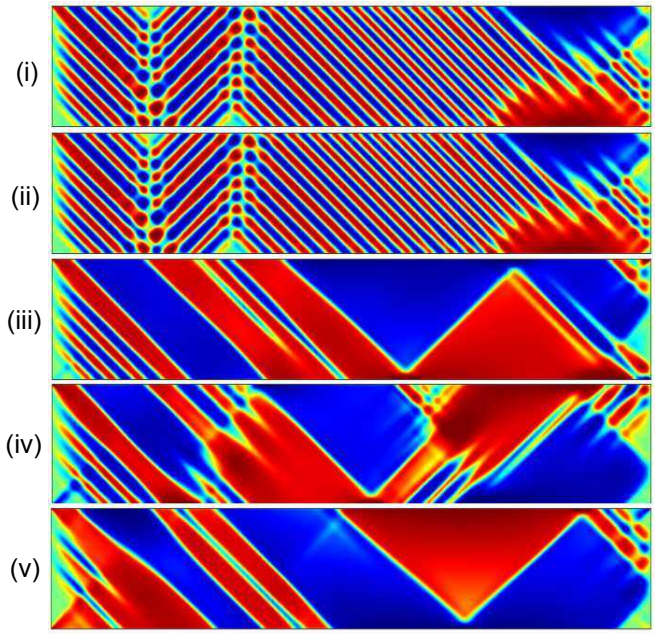

FIGURE 5: (Color online) Evolution of microstructure in the nanowire subjected to bending loading and unloading at time (ns) (i) 0.25, (ii) 0.5, (iii) 1.0, (iv) 1.5, and (v) 2.0 (red and blue indicate martensite variants and green indicates austenite)

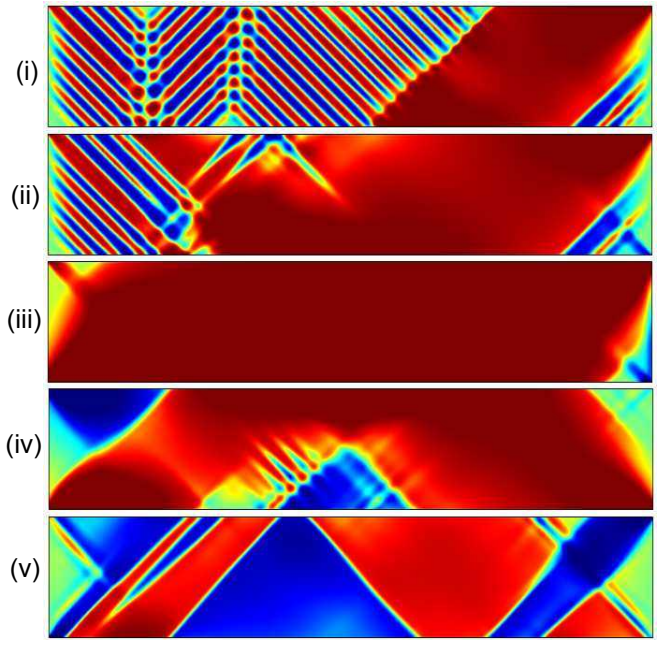

FIGURE 6: (Color online) Evolution of microstructure in the nanowire subjected to multi-axial loading and unloading at time (ns) (i) 0.25, (ii) 0.5, (iii) 1.0, (iv) 1.5, and (v) 2.0 (red and blue indicate martensite variants and green indicates austenite)

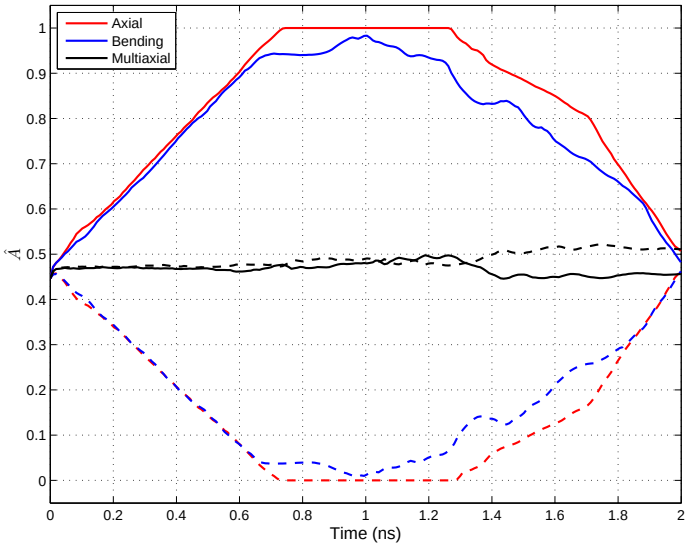

FIGURE 7: (Color online) Evolution of $\hat{A}$ with time for different loading cases (solid lines represent $\hat{A}_{M+}$ and dash lines represent $\hat{A}_{M-}$)

of the bending load, the redistribution of martensite variants is observed with $\hat{A}_{M+}$, and $\hat{A}_{M-}$ values evolving around 0.5. The multi-axial loading case is the combination of axial and bending cases, where the phase transformation and redistribution is occurring simultaneously. This is evident with the fact that $\hat{A}_{M+}$ does not reach value 1 during loading as observed in the axial case.

Figure 8 shows the axial stress-strain behavior of nanowires for the axial and multi-axial case. The dip in the stress at the start of axial loading is due to the sudden disappearance of $M-$ martensitic variant near boundary 4. The detwinning phase transformation and loading occurs simultaneously at around 2.1%, where the whole nanowire is converted to the $M+$ martensite variant. The nanowire responds elastically with steep rise in the stress strain curve after the competition of the detwinning process. The nanowire behavior to the multiaxial loading is stiffer as the axial and bending loads are occurring simultaneously. The elastic loading starts at around 1.8% after the initial phase transformation and loadings.

Figure 9 shows the temperature evolution of different loading cases. It is observed that a constant rate of temperature increase is observed during the phase transformation and simultaneous elastic loading (till 0.7 ns). The rate of temperature rise increases during the elastic loading of the $M+$ variant (0.7 - 1 ns). The movement of twins across boundaries causes an increase in temperature due to friction and the insulated boundary conditions. The waviness and the small drops in the temperature represent the movement of twins across the boundaries and disappearance of twins altogether. During the bending load, the

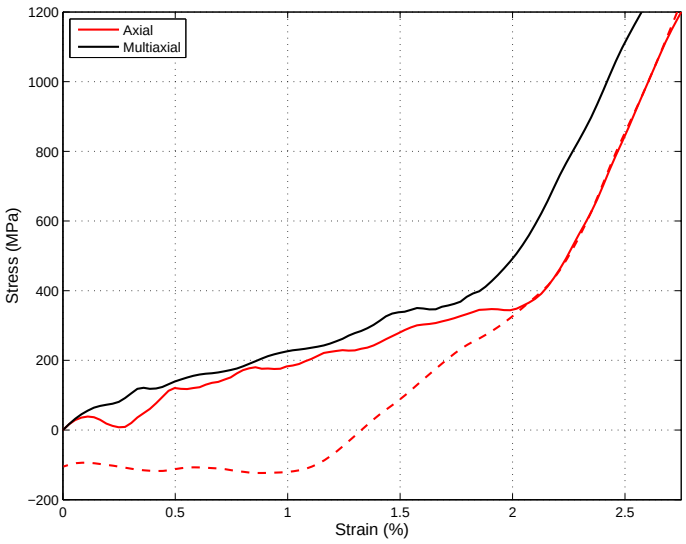

FIGURE 8: (Color online) Average axial stress-strain evolution during axial and multi-axial loadings (solid lines represent loading and dash line represent unloading)

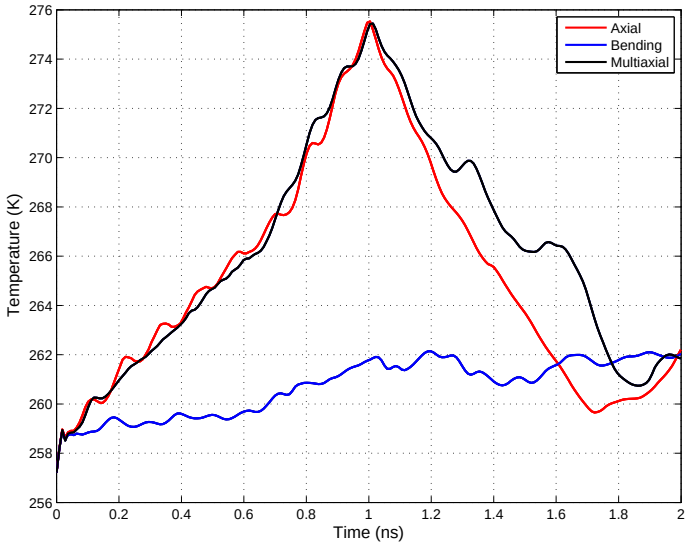

FIGURE 9: (Color online) Temperature evolution during axial and multi-axial loadings (solid lines represent loading and dash line represent unloading)

temperature increase is not steep as observed in the axial case, as the variants are redistributed though the loading and unloading causing the steady rise in a temperature. The multi-axial case is mainly dominated by the axial loading and hence the temperature increase follows the axial case.

CONCLUSIONS

We studied the thermo-mechanical behavior of FePd nanowires under multi-axial loading. The phase field model with the Ginzburg-Landau free energy was used to model the square-to-rectangular phase transformations. The simulations were carried out accounting for the coupled thermo-mechanical physics. The numerical results revealed that the axial loading is dominated by detwinning phase transformation and the bending case by redistribution of martensitic variants based on the local axial stress sign. The multi-axial behavior of nanowire is stiffer axially during loading due to the combination of detwinning and redistribution of the martensitic variants. The multi-axial behaviors can be useful in developing better SMA nanowire based actuators, sensors and control of MEMS and NEMS devices.

ACKNOWLEDGMENT

RD and RM were supported by NSERC and CRC program, Canada.

REFERENCES

[1] Otsuka, K., and Wayman, C., 1998. Shape Memory Materials. Cambridge University Press, New York.

[2] Khovaylo, V., A. Kirilin, V. K., G. Lebedev, V. P., Shavrov, V., and Tulaykova, A., 2008. "New Composite Shape Memory Functional Material for Nano and Microengineering Application". *Proceedings of the 3rd IEEE Int. Conf. on Nano/Micro Engineered and Molecular Systems*, 01, pp. 1231–1236.

[3] Li, M., Tang, H. X., and Roukes, M. L., 2007. "Ultra-sensitive NEMS-based cantilevers for sensing, scanned probe and very high-frequency applications". *Nature Nanotechnology*, ***2***(2), 02, pp. 114–120.

[4] Barcikowski, S., Hahn, A., Guggenheim, M., Reimers, K., and Ostendorf, A., 2010. "Biocompatibility of nanoactuators: stem cell growth on laser-generated NickelTitanium shape memory alloy nanoparticles". *J. Nanopart. Res.*, ***12***(5), pp. 1733–1742.

[5] Yambe, T., Shiraishi, Y., Yoshizawa, M., Tanaka, A., Abe, K., Sato, F., Matsuki, H., Esashi, M., Haga, Y., Maruyama, S., Takagi, T., Luo, Y., Okamoto, E., Kubo, Y., Osaka, M., Nanka, S., Saijo, Y., Mibiki, Y., Yamaguchi, T., Shibata, M., and Nitta, S., 2003. "Artificial myocardium with an artificial baroreflex system using nano technology". *Biomedicine and Pharmacotherapy*, ***57***, pp. 122–125.

[6] Samaroo, H., Lu, J., , and Webster, T., 2003. "Enhanced endothelial cell density on NiTi surfaces with submicron to nanometer roughness". *International Journal of Nanomedicine*, ***3***(1), pp. 75–82.

[7] Khandelwal, A., and Buravalla, V., 2009. "Models for Shape Memory Alloy Behavior: An Overview of Modeling

Approaches". *International Journal of Structural Changes in Solids - Mechanics and Applications,* ***1***(1), pp. 111–148.
[8] Bouville, M., and Ahluwalia, R., 2008. "Microstructure and mechanical properties of constrained shape-memory alloy nanograins and nanowires". *Acta Materialia,* ***56***(14), 08, pp. 3558–3567.
[9] Ahluwalia, R., Lookman, T., and Saxena, A., 2006. "Dynamic Strain Loading of Cubic to Tetragonal Martensites". *MRS Bull.,* ***54***, pp. 2109–2120.
[10] Idesman, A., Cho, J., and Levitas, V., 2008. "Finite Element Modeling of Dynamics of Martensitic Phase Transitions". *Appl. Phys. Lett.,* ***93***(4), p. 043102.
[11] Levitas, V., and Preston, D., 2002. "Three-dimensional Landau theory for multivariant stress-induced martensitic phase transformations. I. Austenite $\leftrightarrow$ martensite". *Physics Review B,* ***66***(134206), pp. 1–9.
[12] Levitas, V., and Preston, D., 2002. "Three-dimensional Landau theory for multivariant stress-induced martensitic phase transformations. II. Multivariant phase transformations and stress space analysis". *Physics Review B,* ***66***(134206), pp. 1–15.
[13] Levitas, V., Preston, D., and Lee, D., 2003. "Three-dimensional Landau theory for multivariant stress-induced martensitic phase transformations. III. Alternative potentials, critical nuclei, kink solutions, and dislocation theory". *Physics Review B,* ***68***(134201), pp. 1–24.
[14] Wang, L., and Melnik, R., 2008. "Modifying Macroscale Variant Combinations in a Two-Dimensional Structure using Mechanical Loadings during Thermally Induced Transformation". *Materials Science and Engineering A, Structural Materials: Properties, Microstructures and Processing*, pp. 190–193.
[15] Wang, L., and Melnik, R., 2008. "Simulation of phase combinations in shape memory alloys patches by hybrid optimization methods". *Applied Numerical Mathematics,* ***58***(4), pp. 511–524.
[16] Onuki, A., 1999. "Pretransitional effects at structural phase transitions". *Journal of the Physical Society of Japan,* ***68***(1), 01, pp. 5–8.
[17] Melnik, R., Roberts, A., and Thomas, K., 2002. "Phase transitions in shape memory alloys with hyperbolic heat conduction and differential-algebraic models". *Computational Mechanics,* ***29***, pp. 16–26.
[18] Melnik, R., Roberts, A., and Thomas, K. A., 2002. "Computing dynamics of Copper-based SMA via center manifold reduction models". *Computational Material Science,* ***18***, pp. 255–268.